Josephson-like Tunnel Resonance and Large Coulomb Drag in GaAs-Based Electron-Hole Bilayers

M. L. Davis,[1] S. Parolo,[1] C. Reichl,[1] W. Dietsche,[1,2] and W. Wegscheider[1,3]
[1]Solid State Physics Laboratory, ETH Zürich, CH-8093 Zürich, Switzerland
[2]Max-Planck-Institut für Festkörperforschung, D-70569 Stuttgart, Germany
[3]Quantum Center, ETH Zürich, CH-8093 Zürich, Switzerland

(Received 13 April 2023; accepted 5 September 2023; published 10 October 2023)

Bilayers consisting of two-dimensional (2D) electron and hole gases separated by a 10 nm thick AlGaAs barrier are formed by charge accumulation in epitaxially grown GaAs. Both vertical and lateral electric transport are measured in the millikelvin temperature range. The conductivity between the layers shows a sharp tunnel resonance at a density of 1.1×10^{10} cm^{-2}, which is consistent with a Josephson-like enhanced tunnel conductance. The tunnel resonance disappears with increasing densities and the two 2D charge gases start to show 2D-Fermi-gas behavior. Interlayer interactions persist causing a positive drag voltage that is very large at small densities. The transition from the Josephson-like tunnel resonance to the Fermi-gas behavior is interpreted as a phase transition from an exciton gas in the Bose-Einstein-condensate state to a degenerate electron-hole Fermi gas.

DOI: 10.1103/PhysRevLett.131.156301

The search for an excitonic Bose-Einstein condensate (BEC) [1] in electron-hole bilayers (EHBs) formed by closely spaced two-dimensional electron and hole gases (2DEGs and 2DHGs, respectively) has been ongoing for some decades [2,3]. It is theoretically predicted to be a superfluid state whose signatures would not only include the dissipationless flow of the excitons but also a Josephson-like enhanced tunneling between the layers and a large Coulomb drag between the layers that persists down to the lowest temperatures [4–13].

The predicted BEC has been the objective of many publications dealing with a large variety of material systems. Both optical excitation and suitable doping in heterostructures have been used to produce excitons [14–19]. Only very recently, some promising results have been reported in two-dimensional atomic layers [20–22]. Additionally, evidence for a condensation has been found in 2DEG bilayers in quantizing magnetic fields [23–25], which is of the Bardeen-Cooper-Schrieffer type [26].

In this Letter we use GaAs-based devices in which the two components of the EHB are separated by a $Al_{0.8}Ga_{0.2}As$ barrier and control the charge densities electrically without optical excitation. We use barriers of only 10 nm thickness, which is considerably thinner than what has been used in earlier experiments [14,18,19,27]. The high quality of our heterostructures allows for the fine-tuning of the charge-carrier densities down to below 1×10^{10} cm^{-2}. At these densities the ratio of Coulomb energy to kinetic energy, usually stated as the r_s value, is sufficiently large to reach the Mott transition between an exciton gas and an electron-hole Fermi gas [8,13,28]. Near the transition we observe a large resonance in the tunnel current between the layers at zero magnetic field indicating a significantly increased tunneling between the electron and the hole layers, reminiscent of the Josephson tunneling observed in the excitonic condensate in 2DEG bilayers in quantizing magnetic fields [23–25]. There, the exciton condensation and the correlation between the two charge layers leads to a dramatic enhancement of the conductivity between the two layers. Our EHBs are different from those of the quantum Hall liquids because the electrons and holes are at different band energies. A Josephson current would be a coherent recombination under the emission of a (coherent) photon as has been discussed by Xie *et al.* [29] for an atomic bilayer system. We also observe an enhanced capacitance, or increased compressibility, in the same density range. This is expected for an exciton condensate as was pointed out by Ma *et al.* [22]. At densities above the Mott transition the EHB transforms into 2D electron-hole Fermi gases that still show indications of Coulomb interaction like a large Coulomb drag between the layers. At even higher densities the mobility vs density traces show novel interaction effects.

The heterostructures investigated in this study were grown by molecular-beam epitaxy. Two undoped GaAs layers separated by a 10 nm $Al_{0.8}Ga_{0.2}As$ barrier are sandwiched between *n*- and *p*-bulk-doped GaAs layers; see Fig. 1(a). Each 2D system, along with its respective doped layer, is contacted separately. Pillar devices with an area of 5.6×10^{-4} cm^2 are used for capacitance and interlayer conductance measurements and have one contact on the top *p* layer, which does not penetrate the barrier. Cross-shaped samples [Fig. 1(b)] have four contacts to both the *n* side and the *p* side, allowing for lateral transport and Coulomb drag measurements. The EHB area of the cross is

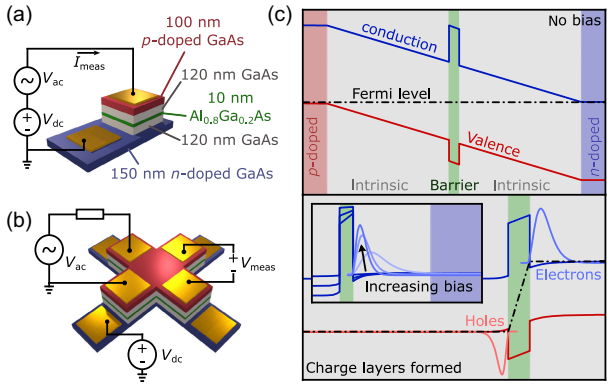

FIG. 1. (a) Schematic of the pillar-shaped sample. The barrier (green) is sandwiched between undoped GaAs spacers. Holes and electrons are provided by p- and n-doped layers at the top and bottom, respectively. (b) Cross-shaped device with four contacts on each doped layer allowing lateral conductivity and frictional drag experiments to be performed on the EHB. (c) Band structure of the devices without a bias (top) and with a bias (bottom). After exceeding the flat-band condition charges accumulate at the barrier. The inset shows the simulated shape of the electron wave function at the barrier. The hole wave function has a similar shape.

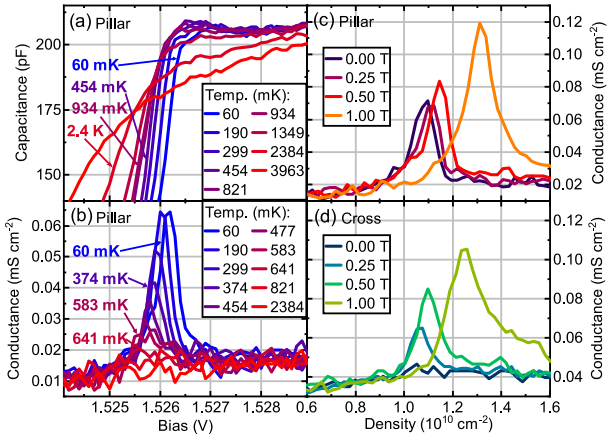

FIG. 2. (a) Temperature dependence of the capacitance shoulder at the onset of mobile charge accumulation. (b) Tunnel resonance of the pillar sample. (c) Tunnel resonance with different magnetic fields applied (pillar sample). (d) Same as (c) but measured on the cross-shaped sample.

8.7×10^{-4} cm^2. Both devices were fabricated from the same growth run. For details of the technology see the Supplemental Material [30]. Applying a dc voltage exceeding that corresponding to the GaAs band-gap energy leads to the flat-band condition and charges accumulate at the barrier, forming the EHB; see Fig. 1(c). Adding a small ac voltage to the dc bias and measuring the in-phase and the out-of-phase components of the resulting ac current yields the tunnel conductance and the capacitance of the EHB, respectively [36].

Measurements of capacitance and conductance are done at the base temperature (20 mK) of a dilution refrigerator. This corresponds to a typical electron temperature of about 60 mK [30]. Results measured at a frequency of 283 Hz and with an ac voltage amplitude of 50 μV are shown in Fig. 2. The capacitance increases steplike at about 1.525 V to values that correspond to a charge-carrier separation of tens of nanometers and signal the existence of an EHB. Beyond the step, the capacitance continues to increase because the shifting of the wave functions leads to a decreasing effective interlayer distance; see Fig. 1(c). The shape of the capacitance vs bias curve does not depend on frequency between 30 Hz and about 3 kHz, indicating that the doped layers and 2D charge gases are in equilibrium in this frequency range. Around the capacitance step, the ordinary tunnel conductance across the barrier is 6 nS, corresponding to a conductivity of 10 μS cm^{-2}. It increases exponentially with increasing bias as expected for Fowler-Nordheim tunneling across a narrow barrier. Resonant tunneling is not expected until much higher biases [37].

Both the capacitance and the tunnel conductance show unusual behavior in this bias region. A shoulder is observed in the capacitance while the tunnel conductance shows a striking resonance. Compared to the ordinary tunnel current across the barrier, the resonance peak is 5 times higher for our predominantly used measurement frequency of 283 Hz, but varies with frequency (see Supplemental Material [30]).

In Figs. 2(a) and 2(b) we plot the temperature dependence of the capacitance and the tunnel resonance, respectively. The capacitance shoulder degrades with increasing temperature and disappears above 2 K, which corresponds to a 100 μeV energy scale, much smaller than typical energies in semiconductors like band offsets and the ionization energies of impurities. The tunnel resonance begins to diminish at a temperature of around 200 mK and continues to do so until it disappears entirely around 1 K. Thus the tunnel resonance exists only in roughly the same temperature range as the capacitance shoulder.

A capacitance enhancement has recently been interpreted as a sign of the increased compressibility that should accompany a BEC state in an EHB [22]. Its occurrence in our samples supports our interpretation that the substantially enhanced conductance across an insulating barrier is a hallmark for Josephson-like charge exchange within an EHB in a condensed state [20,23,38].

Discussing the capacitance and tunneling behavior in the context of condensed excitons requires knowledge of the actual charge densities. The densities of the two 2D charge layers are separately accessible from the Shubnikov–de Haas oscillations of their respective resistances (see the Supplemental Material [30]). The oscillations in the n- and p-doped sides agree with each other, indicating that both 2D charge layers have the same density, as assumed. The densities at biases around 1.53 V are particularly relevant, since this is where the tunnel resonance of Fig. 2 is

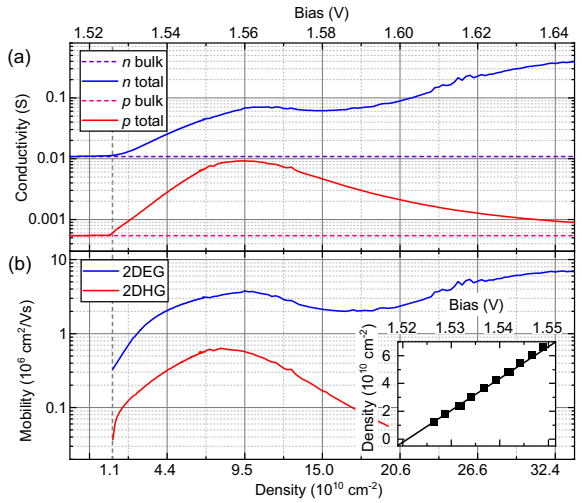

FIG. 3. (a) Conductivities measured on the n- and p-doped sides of the device vs bias voltage. (b) 2DEG and 2DHG mobilities as a function of density. Inset: density vs bias voltage. The dots mark densities obtained from quantum-Hall-effect minima.

observed. This density range is accessible from capacitance vs bias plots in moderate magnetic fields, which show minima at integer fillings of the Landau levels. Thus, the density as a function of bias is precisely determined down to 1.2×10^{10} cm^{-2}. Smaller densities are estimated by extrapolation. A plot of density vs bias at small densities is shown in the inset in Fig. 3.

In Fig. 2(c), the tunnel resonance from Fig. 2(b) is plotted as a function of density. The density at the maximum of the resonance is 1.1×10^{10} cm^{-2} with no magnetic field applied. Also plotted in Fig. 2(c) is the effect of different magnetic fields oriented perpendicular to the EHB plane. The resonance grows and shifts slightly to higher densities with increasing field.

Fogler *et al.* [8] show a zero-temperature phase diagram of an EHB. At small densities (large r_s values) a condensed exciton gas is expected. At larger densities the excitons are expected to separate and form electron and hole Fermi liquids. Under the conditions of our experiments $r_s \approx 8$ and the ratio $d/a_e \approx 6$, which puts our system very near to the expected phase transition between an exciton gas and an electron-hole Fermi liquid. Here, $r_s = (\pi n_e a_e^2)^{-1/2}$, where $a_e \approx 7$ nm is the exciton Bohr radius, n_e is the electron-hole pair density, and d is the effective interlayer distance, which is extracted from band-structure simulations and is 44 nm at the density of the tunnel resonance [39].

The tunnel resonance is also observed in the cross sample from Fig. 1(b), at the same density of 1.1×10^{10} cm^{-2}; see Fig. 2(d). This sample is intrinsically less homogeneous because, in contrast to the pillar, the active area is only partially covered by contact material. This is probably the reason why the tunnel resonance is very weak in zero magnetic field. It nevertheless reaches similar values as in the pillar device already at very moderate magnetic fields (0.25 T).

We identify the tunnel resonance and the capacitance shoulder with a Josephson-like coupling between the electrons and holes in an exciton condensate [20,29]. The length scales are favorable for an exciton gas and a BEC state is expected in the low-temperature limit. Since a BEC requires a sufficiently high density to form at nonzero temperature, one may not be able to see the tunnel resonance at even lower densities. At higher densities a BEC is not possible because of the transition into an electron-hole Fermi gas where the charges behave as a 2DEG adjacent to a 2DHG.

The conductances of the 2D charge gases can be measured in the cross sample. The two doped layers form two crosses superimposed on top of each other. Separate contacts to the ends of the cross arms allow measurement of the conductance per square (or conductivity) of the two crosses separately by the Van der Pauw method. Results are plotted as a function of bias in Fig. 3(a). Clearly, the conductivities of both the n side and the p side increase at about the bias at which the steplike increase of the capacitance is observed. Below this threshold the respective conductivities are almost constant. It is straightforward to subtract the doped layer conductivities and find those of the 2D charge gases. Transport mobilities of both the 2DEG and the 2DHG are plotted in Fig. 3(b).

Both 2D gases show striking mobility maxima that are not observed in standard heterostructures [40,41] nor were they reported in an earlier EHB publication [42]. Mobility peaks of both the 2DEG and the 2DHG occur at a density (9×10^{10} cm^{-2}) at which the average interlayer distance, around 27 nm, is similar to the intralayer distance (≈33 nm) in both layers. Whether or not this is a coincidence will be clarified by future samples with different barrier thicknesses. Although the present devices are not optimized for high mobilities, they reach rather high values—about 7×10^6 cm^2 V^{-1} s^{-1} at a density of about 3.5×10^{11} cm^{-2} for the 2DEG and 0.6×10^6 cm^2 V^{-1} s^{-1} at a density of about 9×10^{10} cm^{-2} for the 2DHG.

In the next part of this Letter, we turn to measurements of frictional, or "Coulomb," drag between the two 2D charge layers. A current I_{drive} flowing along one 2D charge gas of a bilayer system leads to a drag voltage V_{drag} in the second layer due to Coulomb interactions. This is described by the drag resistivity $\rho_D = (W/L) \times (V_{\mathrm{drag}}/I_{\mathrm{drive}})$, with W and L being the length and width of the EHB layers, respectively. In a Fermi gas, the drag effect originates from momentum transfer via scattering processes of the charge carriers, leading to a $\rho_D \propto T^2$ dependence; see, e.g., [43,44]. The magnitude of the drag can be a signature of a BEC state as has been demonstrated for coupled 2DEGs at half-filled Landau levels [45].

We use the cross sample to measure the frictional drag between the 2DEG and the 2DHG. An ac current of 60 nA

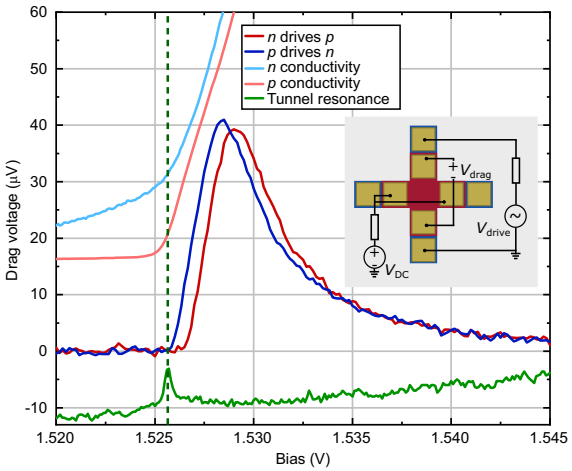

FIG. 4. Drag voltages measured for the n side driving the p side and vice versa. The driving ac current in both cases is 60 nA. Also shown are the tunnel resonance and the conductivities of the n and p layer of the same sample (both in arbitrary units).

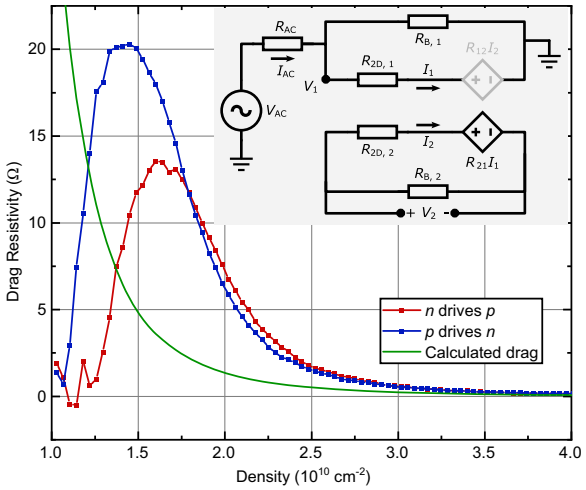

FIG. 5. Intrinsic drag resistivities for the 2DHG driving the 2DEG and vice versa. The green line shows the expected Coulomb drag between two Fermi gases according to the theoretical model. The inset shows the circuit used to extract the intrinsic drag resistivities from the measured drag voltages.

and 13.8 Hz passes straight across one layer while the drag voltage is picked up in the parallel layer; see inset of Fig. 4. A large resistor (100 kΩ) is used in series with the dc voltage source to reduce any ac-current coupling between the two layers via the voltage source [46,47]. Using a significantly smaller or no resistor at all was found to influence the magnitude of the measured drag voltage.

Drag voltages as a function of bias are plotted in Fig. 4. The data show that a positive drag voltage is indeed observed as soon as the 2D gases show an increased conductance as signaled by kinks in the n- and p-layer conductivities. Inverting the drive and the drag layers leads to qualitatively and quantitatively similar curves, in contrast to earlier drag data where significant asymmetries have been observed [18,19]. The signal of the dragged p layer is shifted to slightly higher biases, probably due to the intrinsically lower conductivity of the 2D hole layer compared to the 2DEG. The drag voltages reach maxima at ca. 1.529 V and subsequently decrease with increasing bias. The sign of the drag voltages is positive, which is expected for different polarities in the drag and drive layers. It is significant that the dc bias (and with that the 2D density) at which the steep rise in lateral conductivity occurs coincides not only with the onset of the positive drag voltage but also with the tunnel resonance.

We rule out that the positive drag voltages are caused by the interlayer conductance. An estimate of the expected spurious voltage produced by a network of the p and n layers and the tunnel resistance in the relevant bias regime leads to drag resistances of the order of 10^{-3} Ω.

The measured drag voltages do not correspond directly to the intrinsic drag resistivities between the 2D charge gases because the conducting doped layers modify both the actual current flowing along the drive 2D layer and the measured voltage on the drag side. It follows from a linear network model, see inset of Fig. 5, that the intrinsic drag resistivity (ϱ_D) is related to the measured drag resistance (R_D) by the relation $\varrho_D = R_D \times (W/L) \times (R_{2D,1} + R_{B,1}) \cdot (R_{2D,2} + R_{B,2})/(R_{B,1} \times R_{B,2})$, where $R_{2D,1}$ and $R_{2D,2}$ are the resistances of the 2D drive and drag layers in the EHB, respectively, and $R_{B,1}$ and $R_{B,2}$ those of the two doped layers; see the Supplemental Material [30] for details.

In Fig. 5 the intrinsic drag resistivities are plotted as a function of density, reaching maxima at 13 Ω and 20 Ω. This difference is a result of the correction procedure detailed above; it is not clear if this is intrinsic to the device or if the correction formalism needs to be improved. The solid green line corresponds to the density-dependent Coulomb drag resistivity between two dilute 2D systems expected from theory at 60 mK and adjusted for the interlayer distances in our experimental setup [48]. It is in qualitative agreement with our experimental data for high densities above 4×10^{10} cm^{-2}. Below that, we observe a significantly enhanced drag resistivity as the density is reduced and the 2D layers approach the Mott transition into the excitonic state. The signal peaks at a density of ca. 1.5×10^{10} cm^{-2} and is subsequently cut off due to the very small individual conductivities of the two 2D layers that make the drag experiment impossible.

In conclusion, we prepared high-mobility electron-hole bilayers with barriers of only 10 nm thickness. In these structures we can precisely control densities down to 1×10^{10} cm^{-2}, thus allowing access to the excitonic and the Fermi gas regime of the bilayer system on the low- and high-density side of the Mott transition, respectively. We measure vertical and lateral transport and find, near the Mott transition, a capacitance enhancement and a strongly increased conductance that we interpret as the enhanced

compressibility and the Josephson-like charge transfer in an exciton condensate, respectively. In future experiments, increasing the barrier thickness and applying an in-plane magnetic field will both be used to test their effect on a Josephson coupling. Measuring the counterflow conductance in the excitonic regime could demonstrate excitonic flow that is not yet accessible.

We thank Klaus von Klitzing for illuminating discussions and Peter Märki for sharing his technical expertise and providing valuable support. We acknowledge financial support from the Swiss National Science Foundation (SNSF) and the National Center of Competence in Science "QSIT—Quantum Science and Technology." M. L. D., S. P., and C. R. performed measurements and analysis. M. L. D. and S. P. fabricated the samples and C. R. grew the wafer. W. D. and W. W. conceived of the experiment and interpreted the results. W. D. wrote the manuscript, M. L. D. wrote the Supplemental Material, and C. R. made contributions to both.

[1] J. M. Blatt, K. W. Böer, and W. Brandt, Phys. Rev. **126**, 1691 (1962).
[2] Y. E. Lozovik and V. I. Yudson, Pis'ma Zh. Eksp. Teor. Fiz. **22**, 556 (1975) [JETP Lett. **22**, 274 (1975)].
[3] S. I. Shevchenko, Fiz. Nizk. Temp. **2**, 505 (1976) [Sov. J. Low Temp. Phys. **2**, 251 (1976)].
[4] G. Vignale and A. H. MacDonald, Phys. Rev. Lett. **76**, 2786 (1996).
[5] P. B. Littlewood and X. Zhu, Phys. Scr. **68**, 56 (1996).
[6] C. Zhang and G. Jin, J. Phys. Condens. Matter **25**, 425604 (2013).
[7] A. Perali, D. Neilson, and A. R. Hamilton, Phys. Rev. Lett. **110**, 146803 (2013).
[8] M. M. Fogler, L. V. Butov, and K. S. Novoselov, Nat. Commun. **5**, 4555 (2014).
[9] B. Skinner, Phys. Rev. B **93**, 085436 (2016).
[10] J.-J. Su and A. H. MacDonald, Phys. Rev. B **95**, 045416 (2017).
[11] D. K. Efimkin, G. W. Burg, E. Tutuc, and A. H. MacDonald, Phys. Rev. B **101**, 035413 (2020).
[12] Y. Zeng and A. H. MacDonald, Phys. Rev. B **102**, 085154 (2020).
[13] S. Saberi-Pouya, S. Conti, A. Perali, A. F. Croxall, A. R. Hamilton, F. M. Peeters, and D. Neilson, Phys. Rev. B **101**, 140501(R) (2020).
[14] U. Sivan, P. M. Solomon, and H. Shtrikman, Phys. Rev. Lett. **68**, 1196 (1992).
[15] D. Snoke, Science **298**, 1368 (2002).
[16] L. V. Butov, A. C. Gossard, and D. S. Chemla, Nature (London) **418**, 751 (2002).
[17] H. Deng, G. Weihs, C. Santori, J. Bloch, and Y. Yamamoto, Science **298**, 199 (2002).
[18] J. A. Seamons, C. P. Morath, J. L. Reno, and M. P. Lilly, Phys. Rev. Lett. **102**, 026804 (2009).
[19] A. F. Croxall, K. Das Gupta, C. A. Nicoll, M. Thangaraj, H. E. Beere, I. Farrer, D. A. Ritchie, and M. Pepper, Phys. Rev. Lett. **101**, 246801 (2008).
[20] G. W. Burg, N. Prasad, K. Kim, T. Taniguchi, K. Watanabe, A. H. MacDonald, L. F. Register, and E. Tutuc, Phys. Rev. Lett. **120**, 177702 (2018).
[21] Z. Wang, D. A. Rhodes, K. Watanabe, T. Taniguchi, J. C. Hone, J. Shan, and K. F. Mak, Nature (London) **574**, 76 (2019).
[22] L. Ma, P. X. Nguyen, Z. Wang, Y. Zeng, K. Watanabe, T. Taniguchi, A. H. MacDonald, K. F. Mak, and J. Shan, Nature (London) **598**, 585 (2021).
[23] I. B. Spielman, J. P. Eisenstein, L. N. Pfeiffer, and K. W. West, Phys. Rev. Lett. **84**, 5808 (2000).
[24] E. Tutuc, M. Shayegan, and D. A. Huse, Phys. Rev. Lett. **93**, 036802 (2004).
[25] T. Hyart and B. Rosenow, Phys. Rev. B **83**, 155315 (2011).
[26] D. Zhang, W. Dietsche, and K. von Klitzing, Phys. Rev. Lett. **116**, 186801 (2016).
[27] M. Pohlt, M. Lynass, J. G. S. Lok, W. Dietsche, K. von Klitzing, K. Eberl, and R. Muhle, Appl. Phys. Lett. **80**, 2105 (2002).
[28] D. S. Fisher and P. C. Hohenberg, Phys. Rev. B **37**, 4936 (1988).
[29] M. Xie and A. H. MacDonald, Phys. Rev. Lett. **121**, 067702 (2018).
[30] See Supplemental Material, which includes Refs. [31–35], at http://link.aps.org/supplemental/10.1103/PhysRevLett.131.156301 for heterostructure details, measurement techniques, density and mobility determination, vertical transport frequency dependence, additional drag measurements, and details of the drag correction procedure.
[31] C. Reichl, J. Chen, S. Baer, C. Rössler, T. Ihn, K. Ensslin, W. Dietsche, and W. Wegscheider, New J. Phys. **16**, 023014 (2014).
[32] N. Deng, A. Kumar, M. J. Manfra, L. N. Pfeiffer, K. W. West, and G. A. Csáthy, Phys. Rev. Lett. **108**, 086803 (2012).
[33] J. Nuebler, V. Umansky, R. Morf, M. Heiblum, K. von Klitzing, and J. Smet, Phys. Rev. B **81**, 035316 (2010).
[34] B. N. Narozhny and A. Levchenko, Rev. Mod. Phys. **88**, 025003 (2016).
[35] M. B. Pogrebinskii, Fiz. Tekh. Poluprovodn. **11**, 637 (1977) [Sov. Phys. Semicond. **11**, 372 (1977)].
[36] S. Parolo, M. Lupatini, E. Külah, C. Reichl, W. Dietsche, and W. Wegscheider, Phys. Rev. B **105**, 035304 (2022).
[37] J. J. Finley, R. J. Teissier, M. S. Skolnick, J. W. Cockburn, G. A. Roberts, R. Grey, G. Hill, M. A. Pate, and R. Planel, Phys. Rev. B **58**, 10619 (1998).
[38] L. Tiemann, W. Dietsche, M. Hauser, and K. von Klitzing, New J. Phys. **10**, 045018 (2008).
[39] S. Birner, T. Zibold, T. Andlauer, T. Kubis, M. Sabathil, A. Trellakis, and P. Vogl, IEEE Trans. Electron Devices **54**, 2137 (2007).
[40] J. D. Watson, S. Mondal, G. A. Csáthy, M. J. Manfra, E. H. Hwang, S. Das Sarma, L. N. Pfeiffer, and K. W. West, Phys. Rev. B **83**, 241305(R) (2011).
[41] E. Külah, C. Reichl, J. Scharnetzky, L. Alt, W. Dietsche, and W. Wegscheider, Semicond. Sci. Technol. **36**, 085013 (2021).

[42] C. P. Morath, J. A. Seamons, J. L. Reno, and M. P. Lilly, Phys. Rev. B **78**, 115318 (2008).
[43] A.-P. Jauho and H. Smith, Phys. Rev. B **47**, 4420 (1993).
[44] E. H. Hwang and S. Das Sarma, Phys. Rev. B **78**, 075430 (2008).
[45] J. P. Eisenstein, Annu. Rev. Condens. Matter Phys. **5**, 159 (2014).
[46] K. Das Gupta, A. F. Croxall, J. Waldie, C. A. Nicoll, H. E. Beere, I. Farrer, D. A. Ritchie, and M. Pepper, Adv. Condens. Matter Phys. **2011**, 727958 (2011).
[47] N. P. R. Hill, J. T. Nicholls, E. H. Linfield, M. Pepper, D. A. Ritchie, A. R. Hamilton, and G. A. C. Jones, J. Phys. Condens. Matter **8**, L557 (1996).
[48] E. H. Hwang, S. Das Sarma, V. Braude, and A. Stern, Phys. Rev. Lett. **90**, 086801 (2003).